Volume 1 | Number 1 | Jan 2013 | Pages 1–100

Journal of
Materials Chemistry B

Materials for biology and medicine
www.rsc.org/materialsB

ROYAL SOCIETY
OF CHEMISTRY

ROYAL SOCIETY
OF CHEMISTRY

www.rsc.org/materialsB

Graphical Abstract

The structural role of Zn and its effect on solubility in phosphate based bioglasses is investigated.

1

Structure and solubility behaviour of zinc containing phosphate glasses

N. Kanwal,[a] H. Toms,[a] A.C. Hannon,[b] F.A. Perras,[c] D.L. Bryce,[c] N. Karpukhina[d*] and I. Abrahams[a*]

The structure of phosphate glasses of general composition $10Na_2O:(20 + x/2)ZnO:(20 + x/2)CaO:(50 - x)P_2O_5$ $(0 \leq x \leq 20)$ has been investigated using IR spectroscopy, 1D ^{31}P and ^{43}Ca MAS Bloch decay, $^{31}P-^{31}P$ double quantum MAS-NMR and ^{43}Ca and ^{67}Zn static NMR techniques, as well as neutron diffraction analysis. Zinc is shown to aid glass formation in this system. Glass transition temperature and density increase with increasing cation:phosphate ratio. However, free volume calculations show structures becoming significantly more compact from $x = 5$ to $x = 10$. The structural data confirm depolymerisation of the glasses with increasing cation:phosphate ratio. Zinc oxide is found to act in a network forming role in the system, with ^{67}Zn NMR and neutron diffraction analysis confirming zinc exhibits predominantly four-coordinate geometry. Solubility in deionised water and tris/HCl buffer solution is seen to decrease significantly with increasing x-value. This is discussed in terms of water ingress and the degree of structural openness, associated with increased cross-linking and a decrease in concentration of P−O−P linkages. pH measurements confirm invert phosphate compositions maintain physiological pH levels on immersion in water and buffer solutions for up to four weeks.

2

Introduction

The development of bioresorbable and biocompatible glasses as materials for bone augmentation is of considerable interest due to their ability to form a variety of calcium phosphate based phases, most notably apatite, which chemically resemble the inorganic component of natural bone. In this way, phosphate based glasses have a compositional advantage over existing silicate based systems. However, the fast biodegradation of most phosphate glasses can negate this compositional advantage, with silica based systems often more effective in hydroxyapatite formation. The solubility of phosphate based glasses can be controlled through tailoring of composition,[1-4] allowing for a wide range of potential applications. Additionally, they generally have lower melting points and hence reduced production costs.

Phosphate based biomaterials have been extensively studied and are generally reported to be non-toxic and biocompatible.[5, 6] A number of phosphate based glasses have been studied as potential biomaterials, most notably in the $Na_2O:CaO:P_2O_5$ system.[7, 8] However, these glasses are often very soluble in aqueous media. Various attempts have been made to control the solubility, bioactivity and biocompatibility of these glasses with the incorporation of cations such as Fe^{3+},[9] Ti^{4+},[1, 10] Al^{3+}[11] and Zn^{2+}.[12]

Much work has focussed on metaphosphate glasses, i.e. those containing 50 mol% P_2O_5. In these systems, the glass forming network consists of corner sharing phosphate tetrahedra, with each tetrahedron linked to two other tetrahedra (denoted Q^2) forming long –P–O–P– chains or rings. The bridging P–O bonds are easily hydrolysed in aqueous media and can result in significant lowering of pH, even in the presence of a buffer.[13] Low pH not only inhibits apatite formation, but can also cause demineralisation, an issue that has been widely overlooked. By reducing the phosphate content and increasing the cation content, the degree of polymerisation of the network decreases. However, the network is strengthened as a result of the increase in non-bridging oxygen atoms, through increased cross-linking, particularly involving divalent cations.[14] This results in reduced susceptibility to hydrolysis and hence reduced solubility.

Polyphosphates contain more than one type of phosphate species and readily form in systems containing less than 50 mol% P_2O_5. They generally have a higher affinity to crystallise than metaphosphates. Addition of zinc oxide suppresses crystallisation

3

and extends the glass forming region of polyphosphate glasses.[15] In biomaterials, zinc enhances osteoblast activity and has the potential to be used for the treatment of diseases caused by zinc deficiency, such as rheumatoid arthritis and Crohn's disease. Additionally, zinc is believed to impart antibacterial properties.[16] In the present study, the structure-solubility-composition relationship in a range of zinc containing metaphosphate and polyphosphate glasses is examined, with a view to their potential use as bioresorbable glasses and in composite biomaterials.

Experimental

Preparations

Glasses of general composition $10Na_2O:(20 + x/2)ZnO:(20 + x/2)CaO:(50 - x)P_2O_5$ ($0 \leq x \leq 20$) were prepared by melt quenching methods. Appropriate mixtures of starting materials $NH_4H_2PO_4$ (98-101%), ZnO (99.999%), Na_2CO_3 (99%) and $CaCO_3$ (99%) were ground for 15 min as a slurry in methylated spirits, using an agate mortar and pestle and subsequently dried in air. The dry powder was transferred to a platinum crucible, which was then heated in an electric muffle furnace for 1 h at 300°C to decompose the phosphate, 1 h at 600°C to decompose the carbonate and a further 1 h at a temperature in the range 1100°C to 1350°C to achieve the melt, with higher temperatures required for low phosphate content compositions. The molten glass was quenched rapidly in air in a stainless steel mould to cast discs of 12 mm diameter and 2-3 mm thickness, for solubility studies, or onto a stainless steel plate for bulk glass samples. For glass compositions $x = 15$ and $x = 20$, molten glass was quenched between two stainless steel plates to avoid any surface crystallisation. Glass rods for neutron diffraction experiments were prepared from the molten glass, which was poured into a preheated graphite mould. This was placed into an electric muffle furnace, at a temperature about 20°C above the glass transition temperature, T_g (as measured by DSC), for 1 h. The sample and mould were then cooled slowly in air over a period of *ca*. 24 h. For thermal and structural characterisation studies, the bulk glass samples were ground in an agate mortar to a fine powder. Samples were stored over dry silica gel under vacuum.

4

Diffraction

X-ray powder diffraction (XRD) data were collected on a PANalytical X'Pert Pro diffractometer using Ni filtered Cu-Kα radiation (λ = 1.5418 Å). Data were recorded in flat plate θ/θ geometry over the 2θ range 5 to 70°, at a step width of 0.0334°, with an effective count time of 200 s per step.

Neutron diffraction data were acquired on the General Materials Diffractometer (GEM) at the ISIS Facility, Rutherford Appleton Laboratory, UK.[17] Data were collected on glass rods of approximately 12 mm diameter and 70 mm height. Data were corrected, normalised against a vanadium rod standard and the diffractometer background subtracted using the program Gudrun.[18] Data from banks 2 (13.8-21.0°), 3 (24.8-45.0°), 4 (49.9-74.9°) and 5 (79.0-104.0°) were used to produce the distinct scattering, $i(Q)$, after correction for self-scattering, including a correction for inelastic scattering.[19] The total correlation function, $T(r)$, was obtained by Fourier transformation of $i(Q)$ using the Lorch function,[20] with a maximum momentum transfer of 60 Å^{-1} and fitted up to 3 Å, to obtain pair correlation distances and coordination numbers.[21]

Density measurements

Glass density was measured using a Quantachrome micropycnometer, by displacement of He. Reported results are the average of *ca.* 10 measurements.

Thermal Analysis

A Stanton Redcroft DSC 1500 was used for thermal analysis of the glasses, with powdered alumina used as a reference material. Approximately 50 mg of sample and reference were placed in platinum pans and data recorded over the temperature range 50°C to 1000°C, at a heating rate of 20°C min^{-1}, in an atmosphere of flowing N_2.

Spectroscopy

FTIR spectra were recorded on powdered samples using a Perkin Elmer Spectrum 65 spectrometer, with an ATR attachment. Spectra were recorded over the range 600 to 2000 cm^{-1} and air was subtracted as background.

5

^{31}P MAS-NMR spectra were recorded on a Bruker Avance 600 MHz spectrometer at a resonance frequency of 242.9 MHz. Orthophosphoric acid (85% solution) was used as a reference. Bloch decay spectra were acquired in a 4 mm o.d. zirconia rotor at a spinning speed of 12 kHz. A recycle delay of 60 s was used. A total of 16 scans were acquired for parent glass compositions and 32 scans for samples, post solubility tests. Spectra were modelled using the programs DMFit[22] and NMRLSS.[23] Chemical shift anisotropy parameters were calculated and refined using the Herzfeld–Berger method,[24] with the program HBA.[25] The principal components (δ_{11}, δ_{22}, δ_{33}) of the chemical shift tensor were used to calculate the isotropic chemical shift (δ_{iso}) (Eq.1) and were ordered according to the Haeberlen convention[26]: $|\delta_{33} - \delta_{iso}| > |\delta_{11} - \delta_{iso}| > |\delta_{22} - \delta_{iso}|$.

$$\delta_{iso} = (\delta_{11} + \delta_{22} + \delta_{33})/3 \qquad (1)$$

The chemical shift anisotropy ($\Delta\delta$) and asymmetry (η) parameters are given by:

$$\Delta\delta = \delta_{33} - (\delta_{11} + \delta_{22})/2 \qquad (2)$$

$$\eta = (\delta_{22} - \delta_{11})/(\delta_{33} - \delta_{iso}) \qquad (3)$$

^{31}P–^{31}P double quantum MAS-NMR spectra were collected at a spinning speed of 21 kHz in a 2.5 mm o.d. zirconia rotor, using the Post C7 pulse sequence.[27] To avoid spinning side bands in the ω_1 dimension, t_1 increments were rotor synchronized. A total of 64 t_1 increments were used; each slice was the sum of 16 transients using a recycle delay of 30 s.

[67]Zn and [43]Ca NMR experiments were performed at 21.1 T on a 900 MHz Bruker Avance II spectrometer at the National Ultrahigh-field NMR Facility for Solids in Ottawa, Canada, operating at 56.4 MHz, and 60.56 MHz respectively. [43]Ca experiments were carried out in static and MAS modes (5 kHz spinning speed) on the $x = 15$ composition only, while static [67]Zn data were acquired for all studied compositions. Sample powders were packed into 7 mm o.d. zirconia rotors. Spectra were acquired in a 7 mm home built probe for stationary samples, using the solid echo pulse sequence,[28] with recycle delays of 0.5 s and 1 s for [67]Zn and [43]Ca, respectively. [67]Zn and [43]Ca spectra were referenced to 1 M aqueous solutions of zinc nitrate ($\delta_{iso} = 0$ ppm) and calcium chloride ($\delta_{iso} = 0$ ppm), respectively. Spectra were simulated using the DMFit software.[22]

6

Solubility studies

Solubility of glass discs was measured in deionised water and tris(hydroxymethyl)aminomethane/HCl buffer (tris).[29] The starting pH of the tris buffer solutions was maintained between 7.26 and 7.40. Discs were placed in 25 mL of solution and every seven days discs were removed from solutions, washed with ethanol, dried in an incubator at 80°C for about 15 min, weighed and then immersed in fresh solution. Solutions collected at each time point were filtered through a 0.2 μm syringe filter, stabilised with 0.5 mL of 5% HNO_3 and analysed using a Vista Pro CCD simultaneous ICP-OES. A second set of experiments was carried out, where discs were immersed in 25 mL of solution and left at 37°C for 28 days. The discs were then removed, dried in an incubator at 37°C and ground into a fine powder in an agate mortar. In each case, the powder was then analysed using XRD and ^{31}P MAS-NMR.

Results and discussion

Structure

The XRD patterns for the synthesised glasses are shown in Fig. 1 and reveal that all glasses were amorphous, with no evidence of crystallisation. This contrasts to the situation in the ternary system $NaO:CaO:P_2O_5$, where crystallisation readily occurred in compositions containing 33 mol% P_2O_5 or less.[30] The present results confirm the ability of zinc oxide to aid glass formation in these systems.

The compositional variation of glass transition temperature (T_g), crystallisation temperature (T_c) and glass forming window ($T_c - T_g$) are presented in Fig. 2. T_g increases linearly with increasing x-value, indicating a strengthening of the network with increasing cation:phosphate ratio. This is consistent with observations in sodium and magnesium containing binary phosphate systems, where T_g was also seen to increase with decreasing P_2O_5 content.[30, 31] However, it is different to the trend observed by Walter et al.[32] in binary zinc polyphosphate glasses, with a nominal ZnO content between 50 to 75 mol%, where a minimum in T_g was observed at 60 mol% ZnO. The variation of T_c reflects the wide compositional range studied, from metaphosphates to invert phosphates, and likely reflects a variety of crystalline phases

7

being formed. T_c shows a maximum around $x = 5$. The glass forming window shows a workable range in excess of 100°C for all studied compositions.

A steady increase in density is seen with increasing cation:phosphate ratio in the studied glasses (Fig. 3). The observed density values are consistent with the known density ranges for phosphate glasses.[12] From the density measurements, the percentage free volume (%V_{free}) can be estimated as:

$$\%V_{free} = 100\% \times \left(\frac{V_{FU} - V_{ion}}{V_{FU}} \right) \qquad (4)$$

where V_{FU} is the volume per formula unit and V_{ion} is the calculated ionic volume, which are given by:

$$V_{FU} = \frac{M_r \times 10^{24}}{\rho \, N_A} \, \text{Å}^3 \qquad (5)$$

and

$$V_{ion} = \sum_i n_i \, \tfrac{4}{3} \pi r_i^3 \, \text{Å}^3 \qquad (6)$$

where M_r is the formula unit mass in g mol^{-1}, ρ is the measured density in g cm^{-3}, N_A is Avogadro's constant, n_i is the number of ions of type i per formula unit and r_i is the ionic radius in Å of ion type i according to Shannon.[33] The compositional variation of %V_{free} derived from the density measurements is also shown in Fig. 3. %V_{free} decreases, slightly from $x = 0$ to $x = 5$, with a very significant decrease from $x = 5$ to $x = 10$. At higher values of x, a small increase in %V_{free} is observed. This suggests that while the glass structure becomes slightly more compact from $x = 0$ to $x = 5$, there is a significant compacting of the structure between $x = 5$ and $x = 10$, with higher x-value compositions becoming slightly less compact from $x = 10$ to $x = 20$. This means that the increase in density seen in this latter range is entirely due to the increasing average atomic mass.

It is helpful here to compare the observed trends in density and percentage free volume with those in crystalline zinc phosphates. Table 1 summarises the densities, percentage free volumes and Zn coordination numbers in published crystal structures

8

of zinc phosphates. Average values of density for the different types of Q^n species increase with decreasing level of condensation from ultra- to pyro- phosphate, but change little between ortho- and pyro- phosphates, with values of 3.01, 3.39, 4.03, 4.01 g cm^{-3}, respectively. This is a similar trend to that observed in the present amorphous system and is primarily attributable to the increasing Zn/P ratio, with decreasing level of condensation. Average $\%V_{\text{free}}$ decreases from ultra- to pyro- phosphate, with an increase from pyro- to ortho- phosphate (39.8%, 38.9%, 37.0% and 43.1%, respectively). More significantly, comparison of the percentage free volumes of isocompositional phases with tetrahedrally and octahedrally coordinated zinc shows lower density and $\%V_{\text{free}}$ are associated with the former. In condensed systems this means that the reduced cross-linking of tetrahedrally coordinated zinc, compared to octahedrally coordinated zinc, will result in greater structural openness where zinc adopts the lower coordination number.

Fig. 4 shows the IR spectra for the studied glass compositions. The prominent band at about 1250 cm^{-1}, in the $x = 0$ composition, is attributed to asymmetric stretching of the P=O bond in Q^2 species.[34, 35] This band is seen to loose intensity with increasing x-value and at $x = 20$ is absent. Another strong band at about 900 cm^{-1}, attributed to the P–O–P asymmetric stretch, shifts toward higher wave-number values, with increasing x-value. The bands at around 780 cm^{-1} and 750 cm^{-1} are characteristic of the P–O–P symmetric stretch and P–O–M stretch, respectively.[36] The latter band is seen to become sharper and more prominent in the spectra of higher x-value compositions, consistent with the higher proportion of P–O–M linkages. A small band at 1020 cm^{-1} appears in the spectrum of the $x = 20$ composition, which corresponds to the stretching vibration of the Q^0 (PO_4^{3-}) unit.[37, 38] The weak band observed at 1080 cm^{-1} is related to the asymmetric stretching vibration of PO_3^{2-} species.[39]

The ^{31}P MAS-NMR spectra for the studied glass compositions, recorded at a spinning speed of 12 kHz, are shown in Fig. 5. The spectral parameters derived from fitting these data are presented in Table 2. Resonances with chemical shifts around -25 ppm and a chemical shift anisotropy, $\Delta\delta$, of $ca.$ -150 ppm were assigned to Q^2 phosphate species,[40-42] while those at around -8 ppm, with $\Delta\delta$ values around 130 ppm, were assigned to Q^1 species.[43] The third type of resonance at around 5 ppm was assigned to Q^0 species. The ^{31}P MAS-NMR results are consistent with depolymerisation of the glass with increasing cation:phosphate ratio. The observation of a small amount of Q^0 phosphate as well as Q^1 and Q^2 species in the spectrum for the

9

$x = 15$ composition suggests a small degree of disproportion, consistent with Van Wazer's reorganization theory,[44] or possibly a degree of surface hydrolysis.

Fig. 6 shows ^{31}P–^{31}P double quantum (DQ) MAS-NMR spectra, acquired with the Post C7 pulse sequence, for the studied glass compositions. DQ experiments under MAS allow for determination of through space connectivities between neighbouring Q^n species which have dipole-dipole coupling.[45-48] Peaks on the diagonal (auto-correlated peaks) represent DQ coherences between adjacent units of the same kind, whereas off-diagonal (cross-correlated) pairs correspond to DQ coherences between chemically different groups.[49, 50] For the $x = 0$ glass composition, a single broad auto-correlated peak at *ca.* -25 ppm on the f_2 dimension is attributed to a $Q^{2,2}$ correlation, according to the convention used by Witter *et al.*,[47] where the second exponent refers to the number of bridging oxygen atoms on neighbouring phosphorus atoms. This correlation is consistent with metaphosphate chains or rings.[51] In addition to this correlation, the spectrum of the $x = 10$ composition shows another diagonal peak at about -10 ppm, corresponding to $Q^{1,1}$ correlations. Off-diagonal peak pairs, observed in the spectra for $x = 5$ and 10 compositions, at *ca.* -9 ppm and -27 ppm along the f_2 axis, located at about -35 ppm on the DQ axis, f_1, are associated with $Q^{1,2}$ correlations.[52] The spectrum for the $x = 15$ composition shows an auto correlated Q^1 peak at about -6 ppm on the f_2 axis and chain ending Q^1 units correlated with Q^2 units at around -8 ppm and -20 ppm on the f_2 axis and -28 ppm on the f_1 axis. For the $x = 20$ glass composition, diagonal correlations for $Q^{1,1}$ and $Q^{0,0}$ coherences are observed at about -7 ppm and 5 ppm, respectively, on the f_2 axis. $Q^{1,1}$ being the dominant coherence is an indication of $(P_2O_7)^{4-}$ (Fig. 7a) as the prevailing species in this glass composition. In addition, an off-diagonal correlation pair $Q^{0,1}$ is also observed at about 7 ppm and -8 ppm along the f_2 axis. A similar coherence was observed by Wiench *et al.*[53] in zinc polyphosphate glasses. ^{31}P chemical shift is sensitive to structural changes up to the fourth coordination sphere of phosphorus.[47, 51, 54]

Quantitative measurement of the different species detected in the DQ experiments is not straightforward. However, this can be achieved by quantitative fitting of the 1D MAS-NMR spectra, with chemical shift and line width for each of the correlating species determined from the DQ MAS spectra. Table 3 presents the proportion of each of the correlated species calculated by fitting the 21 kHz 1D spectra. The total percentage Q^n speciation values were within 5% of the

10

corresponding values from direct fitting of the 12 kHz data (Table 2). As mentioned above, DQ experiments under MAS with the Post C7 pulse sequence are sensitive to through space dipolar couplings. When considering the quantitative results it is therefore important to consider the possible contribution of correlations between Q^n species that may not be directly bonded as well as those that are directly bonded. To assess this, it is helpful to compare the relative integrals of cross Q^n coherences (Table 3) with those derived for the individual species from the 1D 12 kHz data (Table 2). Since Q^2 units must bridge two phosphate units, they can only be present in the system as part of a ring or chain, involving three or more phosphate tetrahedra. However, Q^1 species may be present as $(P_2O_7)^{4-}$ dimers, as chain ends or as part of a polyphosphate anion. In order to distinguish these, the integral of the $Q^{1,2}$ coherence needs to be compared to that of the total Q^1 species in the 1D 12 kHz pattern. If the two numbers are approximately equal then it can be concluded that all or most of the Q^1 species are chain ends (where a chain contains at least three phosphate tetrahedra) and that there is a minimal contribution to the total $Q^{1,2}$ coherence from Q^2 species on adjacent chains. This is true only in the case of the $x = 5$ glass composition. In that composition, the integral of the $Q^{1,2}$ coherence is 15.7 %, which compares with a value of 17.9% for the total Q^1 species from the analysis of the 1D data and confirms a minimal contribution to the 2D pattern of correlated Q^n species that are not directly bonded. 69.3% $Q^{2,2}$ correlations are found and correspond to Q^2 units within long chains or rings. The remaining Q^2 species (15.0%) are terminated by an approximately equal number of Q^1 units, indicating a chain length greater than or equal to four phosphate polyhedra. For the $x = 10$ and $x = 15$ compositions, integration of the 1D 12 kHz spectrum shows significantly more Q^1 species than can be attributed to chain ends (i.e. much larger than the $Q^{1,2}$ integral). This means that the remaining Q^1 species can only be linked to other Q^1 species, i.e. as the $(P_2O_7)^{4-}$ dimer. This is confirmed by the sum of the $Q^{1,2}$ and $Q^{1,1}$ integrals, which is very close to the total Q^1 integral found in the conventional 1D spectral analyses. The $x = 10$ glass composition shows a distribution of three different kinds of species, with 26.8% $Q^{1,1}$ dimers, 22.1% $Q^{2,2}$ long chain or rings and 25% of Q^2 species which are linked to Q^1 species. The $x = 15$ glass composition has 56.9% $Q^{1,1}$ dimer units, with ca. 21% Q^2 linked to chain end Q^1 species. The absence of $Q^{2,2}$ correlations for this latter composition suggests trimeric species of the type $(P_3O_{10})^{5-}$ (Fig. 7b). The $x = 20$ glass composition has 72.5% $Q^{1,1}$ species corresponding to pyrophosphate units, 6.8% $Q^{0,0}$ species and about 10% of Q^1 species coupled to an equal quantity of Q^0 species.[50] In this case, the

11

presence of correlations involving Q^0 can only be accounted for by through space coupling of species not directly bonded to each other. The projections from the 2D spectra only show correlated species and hence not all the Q^0 species are represented.

^{67}Zn NMR spectra are presented in Fig. 8. Each spectrum was fitted using a distribution of chemical shifts and quadrupolar coupling constants using the Czjzek model as implemented in the DMFit software.[22,55] This model uses a Gaussian distribution of δ_{iso} and C_Q values to properly represent the variability in local glass structure. The ^{67}Zn NMR spectra are very well fitted using a single average glass site for each sample (see Fig. 8). The values of C_Q are essentially constant at 7.4 to 8.0 MHz, with a distribution on each value of 0.5 MHz. The chemical shifts cover only a small range, from 150 to 235 ppm (each with a distribution of 50 ppm). The values obtained from the fits (Table 4) are therefore consistent with zinc in a predominantly four-coordinate pseudo-tetrahedral geometry in all samples.[56-61]

^{43}Ca static and MAS-NMR spectra for the $x = 15$ glass composition are presented in Fig. 9. The line shape of the static spectrum is typical of a disordered structure. Although the line width decreases when the sample is spun at 5 kHz, the spectrum could not be resolved into more than one resonance, suggesting significant chemical shift distribution, as expected in a glass. The moderate signal-to-noise and lack of clear line shape features preclude a precise fitting of the ^{43}Ca MAS NMR spectrum; however, we can report a peak position of -1 ppm and an upper limit of 4.7 MHz for the value of C_Q. These values fall within the ranges seen for crystalline calcium phosphates.[62, 63]

The total correlation functions $T(r)$, obtained from the neutron scattering data on the studied compositions are shown in Fig. 10. $T(r)$ for all compositions was fitted using resolution-broadened Gaussian peaks;[21] that for the $x = 5$ composition is typical and is shown in Fig. 11, with the fits to the data for the other compositions available as supplementary data (Figs S1 to S4). Two short P–O correlations were resolved at about 1.5 Å (corresponding to P–NBO) and *ca*. 1.6 Å (corresponding to P–BO). P-O distances are plotted as a function of composition in Fig 12. The P–NBO bond length increases with increasing cation:phosphate ratio. The P–BO bond length is seen to decrease from $x = 0$ to $x = 5$, but then shows a small but steady increase above $x = 5$. Additionally, the P–BO peak becomes broader and decreases in intensity, indicative of the change in the level of condensation with increasing metal oxide content.[64] Table 5 summarises the derived pair correlations and coordination numbers for the studied compositions. The O–O coordination number for each glass composition was calculated according to the formula $24/(5 + y)$,[65] where y is the mole ratio between mole

12

fraction of modifier and phosphate content. The $T(r)$ peak at about 2.5 Å was fitted according to the calculated coordination number and subtracted from the rest of the $T(r)$. The fit of the residual area between 1.75 Å to 2.75 Å gives the coordination numbers for Zn–O and Na/Ca––O. A prominent peak at ~1.9 Å is observed in the $T(r)$ plots for all compositions, which increases in intensity with increasing zinc content. The Zn–O coordination numbers range from 3.9 to 4.3 and are consistent with predominantly four coordinate geometry for zinc, as observed in other studies of zinc phosphate glasses[32, 66, 67] and are in agreement with the [67]Zn NMR results. The slightly higher values for some compositions could be an indication of a small proportion of zinc in six coordinate geometry, as found through X─ray and neutron diffraction of zinc phosphate systems by Suzuya *et al.*[68]. Indeed, a second weak Zn-O correlation at 2.17 Å was discernible in the data for the $x = 20$ composition which is attributed to Zn in six coordinate geometry. An average coordination number of around seven is observed for the unresolved Na/Ca–O peak. The average Na/Ca-O correlation distance is seen to vary little with composition, despite the increasing Ca:Na ratio with increasing x-value.

Solubility

Changes in pH values in tris buffer and deionised water are plotted as a function of immersion time in Fig. 13. In tris buffer, all samples showed a minimum in pH after two weeks immersion. Only the $x = 0$ glass composition showed significant deviation away from pH = 7 to lower pH, with a minimum value of pH = 6.5. In deionised water, the $x = 0$ and $x = 5$ compositions showed a decrease in pH, which was maintained in fresh solutions up to week 3, with a small increase in week 4. For the less condensed samples $x = 10$ to $x = 20$ an increase in pH was observed after immersion for a week. For the $x = 10$ composition, the pH of fresh solutions, showed a small, but steady, decrease for the duration of the experiment. In contrast, for composition $x = 15$, the pH of fresh solutions was almost constant until week 3, showing a small decrease between weeks 3 and 4, while that for the $x = 20$ composition remained almost constant throughout the experiment. The observed changes in pH reflect the corresponding weight loss profiles shown in Fig. 14, which reveal decreasing weight loss with decreasing level of condensation, indicating that the $x = 0$ composition is the most soluble, while the $x = 10$, 15 and $x = 20$ compositions show very limited solubility. While increasing solubility with increasing level of

condensation appears to be counter intuitive, it is an established phenomenon in phosphate glasses.[1,69]

The solubility results seen here reflect the changes in percentage free volume and density seen in Fig. 3, with the glass with the highest solubility having the highest $\%V_{\text{free}}$ and lowest density. This suggests that the greater structural openness of the of $x = 0$ and $x = 5$ compositions (as reflected in the percentage free volume) allows for more rapid water ingress and hence greater solubility, despite exhibiting the greatest degree of P-O-P condensation. As discussed above, evidence from crystalline phosphates shows that percentage free volume is only weakly associated with the level of P-O-P condensation, being more significantly affected by the coordination adopted by zinc and hence the extent of cross-linking. Thus, the higher free volume and more openness of the low x-value glass compositions may well be associated with a greater proportion of tetrahedral zinc, compared to the high x-value compositions.

XRD patterns for the glass discs after immersion in tris buffer for 28 days are presented in Fig. 15. Sharp Bragg peaks are only observed in the glass composition $x = 0$, whereas the absence of Bragg peaks in the patterns of the other compositions confirms their amorphous nature. The diffraction peaks in the pattern for the $x = 0$ composition are consistent with a mixture of hydrated zinc and calcium pyrophosphates ($Zn_2P_2O_7.3H_2O$, JCPDS 11-22; $Ca_3H_2(P_2O_7)_2.4H_2O$, JCPDS 44-810).

^{31}P MAS-NMR spectra of glass discs after immersion in tris buffer for 28 days are presented in Fig. 16. The presence of sharp peaks at about -4 ppm and -7 ppm for glass composition $x = 0$ is consistent with the precipitation of crystalline pyrophosphates, with some residual amorphous metaphosphate phase. Glass composition $x = 5$ shows a significant increase in Q^1 species and decrease in Q^2 species, with the formation of an additional amorphous Q^0 species. For all other glass compositions, no major change is observed compared to the spectra of the glasses before immersion. These changes reflect the relative solubilities of the glass compositions in tris buffer (Fig. 14b).

Ion release profiles in tris buffer and deionised water, for constituent ions, in all studied glass compositions, as a function of time are shown in Fig. 17 as 3D plots. It is evident from the figures that the amount of ions released upon dissolution of discs in both tris buffer and distilled water decreased with decreasing phosphate content and increasing cation content, reflecting the weight loss and pH measurements. In the most soluble glass composition, $x = 0$, for each ion studied, a large initial release of ions was observed at week 1, which decreased to a near steady state after week 1 up to

14

week 3 and then increased again in week 4 in deionised water. For this glass composition in tris buffer, a steady decrease in ion release was observed for all ions except Zn^{2+}, which remained fairly constant for three weeks, before decreasing in week 4. Glass compositions $x = 5$ and 10 showed nearly the same behaviour in both studied media, with an initial increase and then decrease in weight loss of all constituent ions. For the $x = 0$ and $x = 5$ compositions, it is evident that there is significant loss of phosphate as well as other ions in both media. For the $x = 5$ composition this feature, along with the change in Q^n speciation in the glass after immersion in tris buffer (Fig. 16), is a good indication of network cleavage (i.e. hydrolysis of P−O−P linkages) taking place in the dissolution process. For the two most condensed compositions there was very little ion release in deionised water and tris buffer. However, higher weight loss and ion release were observed for glass compositions $x = 10$, 15 and 20 in tris buffer than in deionised water, while the reverse was true for glass compositions $x = 0$ and 5.

The dissolution of phosphate glasses is considered to proceed through two basic processes, which involve the ingress of water or protons at the glass surface:[70]

(i) Ion exchange

$$(7)$$
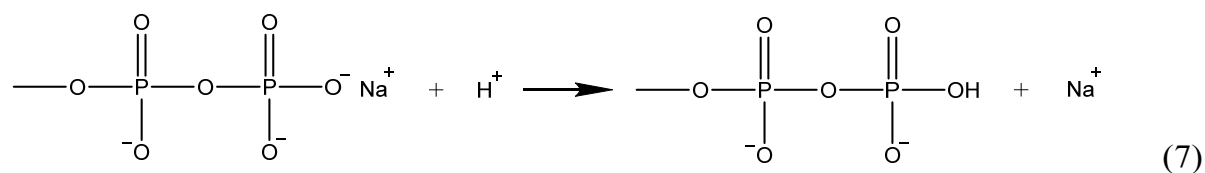
(ii) Network cleavage

$$(8)$$
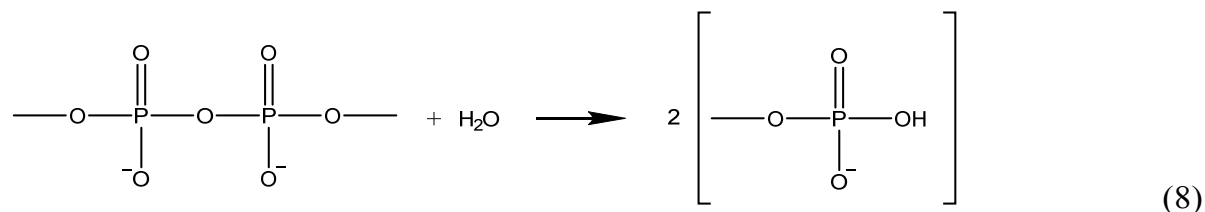
There has been much discussion as to which of these processes dominates the dissolution process. Bunker et al.[70] found ion exchange to be the more dominant reaction. This results in phosphate species in solution with similar average chain lengths to the parent glass. However, later work found the network cleavage reaction

15

also to be critical.[71] Network cleavage results in phosphate species in solution with a variety of chain lengths, generally smaller than in the parent glass. pH has also been found to be an important factor, with P–O–P linkages highly susceptible to proton attack.[70,71] Using solution state NMR, Döhler et $al.$[69] have recently shown that the mechanism of dissolution adopted in phosphate glasses, depends on the level of condensation, with glasses containing chains (predominantly Q^2) dissolving mainly by ion exchange, and those containing Q^3 species dissolving by network cleavage.

The higher solubility of the lower x-value compositions may be explained by considering their structures, as determined by Bloch decay and DQ ^{31}P MAS-NMR spectroscopy. In the studied compositions, the cation:phosphate ratio increases with increasing x-value. This results in increased cross-linking and a strengthening of the network with increasing cation content.[14, 70] Phosphate glasses with increased amounts of divalent cations, such as Ca^{2+}, show reduced solubility, which is believed to be mainly due to the increased cross-linking effect.[30] In the present system, the structure of the $x = 0$ composition consists of long –P–O–P– chains or rings, with a low degree of P–O...M cross-linkages, while that for the $x = 5$ composition contained long chains, short chains and a very small proportion of dimer units. Additionally, these compositions show the highest values of $\%V_{free}$ allowing for more rapid water ingress. As discussed above, the P–O–P linkage is very susceptible to attack by protons (H^+), with decreasing pH increasing dissolution.[71] However, H^+ ions are buffered in tris solution and hence the dissolution rate slows down. The $x = 5$ glass composition releases half the amount of phosphate ions in tris buffer compared to the $x = 0$ composition, mainly because there are more P–O...M linkages and fewer P–O–P linkages, $i.e.$ greater cross-linking compared to the $x = 0$ composition. A significant decrease in solubility occurs in changing composition from $x = 5$ to $x = 10$. The $x = 10$ glass releases about 2.4 times less phosphate ions than the $x = 5$ glass due to the higher degree of depolymerisation, greater cross-linking, presence of a large proportion of dimer (pyrophosphate) units and most significantly the dramatic decrease in percentage free volume. As x increases further, the dissolution rate continues to decrease. The $x = 15$ glass composition releases phosphate ions only 1.5 times less than the $x = 10$ composition, with the $x = 20$ glass composition virtually insoluble. For these higher x-value compositions the results suggest that the decrease in solubility

16

with increasing *x*-value is predominantly associated with the increase in cross-linking (*i.e.* P–O…M linkages) and the decrease in concentration of P–O–P linkages.

The ion release profiles show the amount of zinc released is higher than that for calcium in glasses with low or no Q^2 species (*i.e.* x = 10, 15 and 20), when immersed in deionised water. However, in tris buffer the concentration of calcium released is always higher than zinc for all glass compositions. This indicates that more zinc is released in acidic pH, which is in agreement with other studies carried out on zinc containing silicate glasses.[72] The higher degradation of compositions x = 10, 15 and 20 in tris buffer than in deionised water contrasts the behaviour of the x = 0 and 5 compositions and can be explained by Bunker's theory.[70] The degradation of phosphate glass occurs by the uptake of both H^+ and OH^- ions from solution and for pH below 6.5 uptake of H^+ is higher, whereas at pH values above 6.5 OH^- is consumed more. For these glass compositions, where P–O–P bonds are not available for H^+ uptake in deionised water, there is a greater uptake of OH^- ions in tris buffer and hence more dissolution. This is also indicated by the increase in pH of the solutions for these compositions. In addition, the degradation of small chains and cyclic rings decreases in acid medium and increases in basic solution, which explains the lower dissolution of the x = 10 and 15 compositions, due to the presence of such short chains, as observed in the ^{31}P DQ NMR experiments. The observed changes in pH for the metaphosphate composition are fairly consistent with the results of Ahmed *et al.*,[8] who studied sodium calcium phosphate glass dissolution. However, for compositions around 45 mol% P_2O_5 (corresponding to x = 5 in the present study) these authors reported an increase in pH for sodium calcium phosphate glasses, compared to the decrease seen in the present study. This difference can only be attributed to the presence of zinc in the current study.

In solubility studies of zinc substituted sodium calcium metaphosphate glasses, Salih *et al.*[73] observed the highest degradation rate and lowest pH for glass compositions containing the highest amount of zinc. Evidence in the present study suggests a predominantly network forming role for ZnO in this system, with the presence of ZnO_4 tetrahedra between PO_4 tetrahedra. This suggests that the Zn-O bond in these systems is significantly covalent in nature. A simple calculation of ionic character based on Pauling's scale of electronegativity,[74] yields a value of 55% ionic character for Zn-O compared to values of 32%, 77% and 79% for P-O, Ca-O and Na-O, respectively. Indeed, *ab initio* calculations on ZnO clusters show ionic and covalent

17

models describe the system equally well.[75] ZnO is well known to be soluble in dilute acids [74] and it is therefore possible that degradation of Zn–O–P linkages occurs in a similar way to the degradation of P–O–P linkages. Thus, the higher degradation rate of zinc containing metaphosphate glasses described by Salih *et al.* indicates susceptibility of the Zn−O−P linkage to proton attack, increasing the degradation rate and decreasing pH.

Conclusions

In agreement with other studies, inclusion of zinc oxide in sodium calcium phosphate glasses is shown to aid glass formation. A strengthening of the glass network is observed with increasing cation:phosphate ratio, which is accompanied by an increase in density. However, calculations of percentage free volume indicate that this increase is due to increasing average atomic mass, with glasses becoming slightly less compact at higher cation:phosphate ratios.

Structural data are consistent with depolymerisation of these glasses with increasing cation:phosphate ratio, with greater numbers of non-bridging oxygen atoms in higher x–value compositions. ^{31}P–^{31}P DQ MAS-NMR has been used to reveal detail of the connectivity of Q^n species in the studied glasses and reveals evidence for the network forming role of zinc oxide. This is confirmed by neutron diffraction and ^{67}Zn NMR analyses which show zinc to be in predominantly four-coordinate geometry.

The solubility of the studied glasses, decreases with increasing cation:phosphate ratio. At low cation:phosphate ratios, high solubility is predominantly associated with the degree of openness of the glass structure allowing for rapid water ingress. This structural openness is partly attributed to the low coordination number of zinc resulting in low cross-link density. At higher cation:phosphate ratios, where percentage free volume is significantly lower, solubility is low due to the compactness of the structure with increased cross-linking and lower concentrations of P−O−P linkages. Evidence in the neutron diffraction data suggests the role of zinc changes with composition, with a proportion of the zinc adopting a higher coordination number in the sample with the highest cation:phosphate ratio and therefore exhibiting higher cross-linking density. Metaphosphate glasses, with more open structures containing high concentrations of longer chains or rings, show high solubility and greater ion release, while invert phosphate glasses, with low phosphate content and more compact

18

structures, show only limited solubility in deionised water and buffer solution. The invert phosphate glasses maintain pH levels within the physiological range on immersion, which is an important consideration for biomedical applications.

Acknowledgements

Notes and references

[a] Materials, Research Institute, School of Biological and Chemical Sciences, Queen Mary University of London, Mile End Road, London E1 4NS, UK.

[b] STFC ISIS Facility, Rutherford Appleton Laboratory, Chilton, Didcot, Oxfordshire, OX11 0QX, UK.

[c] Department of Chemistry, Centre for Catalysis Research and Innovation, University of Ottawa, 10 Marie Curie Private, Ottawa, Ontario, Canada K1N 6N5.

[d] Barts and the London School of Medicine and Dentistry, Queen Mary University of London, Mile End Road, London E1 4NS, UK.

1.   D. S. Brauer, C. Ruessel and J. Kraft, *J. Non-Cryst. Solids*, 2007, **353**, 263-270.

2.   K. Franks, V. Salih, J. C. Knowles and I. Olsen, *J. Mater. Sci.-Mater. M.*, 2002, **13**, 549-556.

3.   M. Bitar, J. C. Knowles, M. P. Lewis and V. Salih, *J. Mater. Sci.-Mater. M.,* 2005, **16**, 1131-1136.

4.   M. Navarro, M. P. Ginebra and J. A. Planell, *J. Biomed. Mater. Res.-A*, 2003, **67A**, 1009-1015.

19

5.   A. Ito, M. Otsuka, H. Kawamura, M. Ikeuchi, H. Ohgushi, Y. Sogo and N. Ichinose, *Curr. Appl. Phys.*, 2005, **5**, 402-406.

6.   S. N. Silva, M. M. Pereira, A. M. Goes and M. F. Leite, *J. Biomed. Mater. Res.-A*, 2003, **65A**, 475-481.

7.   I. Ahmed, M. Lewis, I. Olsen and J. C. Knowles, *Biomaterials*, 2004, **25**, 501-507.

8.   I. Ahmed, M. Lewis, I. Olsen and J. C. Knowles, *Biomaterials*, 2004, **25**, 491-499.

9.   E. A. Abou Neel, I. Ahmed, J. J. Blaker, A. Bismarck, A. R. Boccaccini, M. P. Lewis, S. N. Nazhat and J. C. Knowles, *Acta Biomaterialia*, 2005, **1**, 553-563.

10.   N. J. Lakhkar, J.-H. Park, N. J. Mordan, V. Salih, I. B. Wall, H.-W. Kim, S. P. King, J. V. Hanna, R. A. Martin, O. Addison, J. F. W. Mosselmans and J. C. Knowles, *Acta Biomaterialia*, 2012, **8**, 4181-4190.

11.   I. Abrahams, K. Franks, G. E. Hawkes, G. Philippou, J. Knowles, P. Bodart and T. Nunes, *J. Mater. Chem.*, 1997, **7**, 1573-1580.

12.   E. A. Abou Neel, L. A. O'Dell, M. E. Smith and J. C. Knowles, *J. Mater. Sci.-Mater. M.*, 2008, **19,** 1669-1679.

13.   G. Novajra, C. Vitale-Brovarone, J. C. Knowles, G. Maina, V. Aina, D. Ghigo and L. Bergandi, *J. Biomed. Mater. Res.-A*, 2011, **99A**, 295-306.

14.   J. R. Van Wazer and D. A. Campanella, *J. Am. Chem. Soc*, 1950, **72**, 655-663.

15.   K. Suzuya, K. Itoh, A. Kajinami and C. K. Loong, *J. Non-Cryst. Solids*, 2004, **345,** 80-87.

16.   O. Clarkin, A. Wren, R. Thornton, J. Cooney and M. Towler, *J. Biomater. Appl* 2011, **26**, 277-292.

17.   A. C. Hannon, *Nucl. Instrum. Meth. A*, 2005, **551**, 88-107.

18.   A. K. Soper, *GudrunN and GudrunX : programs for correcting raw neutron and X-ray diffraction data to differential scattering cross section*, Report RAL-TR-2011-013, Rutherford Appleton Laboratory Technical, 2011.

19.   A. C. Hannon, W. S. Howells and A. K. Soper, *Inst. Phys. Conf. Ser.*, 1990, **107**, 193-211.

20.   E. Lorch, *J. Phys. C*, 1969, **2**, 229-237.

21.   A. C. Hannon, PFIT correlation function fitting software, http://www.alexhannon.co.uk/.

20

22.   D. Massiot, F. Fayon, M. Capron, I. King, S. Le Calvé, B. Alonso, J. O. Durand, B. Bujoli, Z. H. Gan and G. Hoatson, *Magn. Reson. Chem*, 2002, **40**, 70-76.

23.   NMRLSS - Nuclear Magnetic Resonance Least Squares Refinement for Solids, Version 1.5, I. Abrahams, Queen Mary University of London, 2003.

24.   J. Herzfeld and A. E. Berger, *J. Chem. Phys.*, 1980, **73**, 6021-6030.

25.   HBA Version 1.7, K. Eichele, Universität Tübingen, 2012

26.   U. Haeberlen, *Advances in Magnetic Resonance*, Academic Press, New York, 1976.

27.   T. Karlsson, J. M. Popham, J. R. Long, N. Oyler and G. P. Drobny, *J. Am. Chem. Soc.*, 2003, **125**, 7394-7407.

28.   J. T. Cheng and P. D. Ellis, *J. Phys. Chem.,* 1989, **93**, 2549-2555.

29.   M. Mneimne, R. G. Hill, A. J. Bushby and D. S. Brauer, *Acta Biomaterialia*, 2011, **7**, 1827-1834.

30.   M. Uo, M. Mizuno, Y. Kuboki, A. Makishima and F. Watari, *Biomaterials*, 1998, **19**, 2277-2284.

31.   G. Walter, J. Vogel, U. Hoppe and P. Hartmann, *J. Non-Cryst. Solids*, 2003, **320**, 210-222.

32.   G. Walter, U. Hoppe, J. Vogel, G. Carl and P. Hartmann, *J. Non-Cryst. Solids*, 2004, **333**, 252-262.

33.   R.D. Shannon, *Acta Crystallogr*., 1976, **A32**, 751-767.

34.   G. Le Saout, P. Simon, F. Fayon, A. Blin and Y. Vaills, *J. Raman Spectrosc.*, 2002, **33**, 740-746.

35.   A. Saranti, I. Koutselas and M. A. Karakassides, *J. Non-Cryst. Solids*, 2006, **352**, 390-398.

36.   D. Boudlich, L. Bih, M. E. Archidi, M. Haddad, A. Yacoubi, A. Nadiri and B. Elouadi, *J. Am. Ceram. Soc.*, 2002, **85**, 623-630.

37.   D. Muresan, M. D. Bularda, C. Popa, L. Baiai and S. Simon, *Romanain J. Phys.*, 2006, **51**, 231-237.

38.   H. S. Gao, T. N. Tan and D. H. Wang, *J. Control. Release*, 2004, **96**, 21-28.

39.   G. Le Saout, P. Simon, F. Fayon, A. Blin and Y. Vaills, *J J. Raman Spectrosc.*, 2009, **40**, 522-526.

40.   R. K. Brow, *J. Non-Cryst. Solids*, 2000, **263**, 1-28.

41.   R. J. Kirkpatrick and R. K. Brow, *Solid State Nucl. Mag. Reson.*, 1995, **5**, 9-21.

42.   R. K. Brow, C. C. Phifer, G. L. Turner and R. J. Kirkpatrick, *J. Am. Ceram. Soc.*, 1991, **74**, 1287-1290.

43.   G. Walter, J. Vogel, U. Hoppe and P. Hartmann, *J. Non-Cryst. Solids*, 2001, **296**, 212-223.

44.   J. R. Van Wazer, *Phosphorus and its compounds*, Interscience, New York, 1958.

45.   H. Geen, J. Gottwald, R. Graf, I. Schnell, H. W. Spiess and J. J. Titman, *J. Magn. Reson.*, 1997, **125**, 224-227.

46.   M. Feike, C. Jager and H. W. Spiess, *Journal of Non-Crystalline Solids*, 1998, **223**, 200-206.

47.   R. Witter, P. Hartmann, J. Vogel and C. Jager, *Solid State Nucl. Mag. Reson*, 1998, **13**, 189-200.

48.   C. Jager, P. Hartmann, G. KunathFandrei, O. Hirsch, P. Rehak, J. Vogel, M. Feike, H. W. Spiess, K. Herzog and B. Thomas, *Ber. Bunsen Phys. Chem.*, 1996, **100**, 1560-1562.

49.   M. Feike, R. Graf, I. Schnell, C. Jager and H. W. Spiess, *J. Am. Chem. Soc.*, 1996, **118**, 9631-9634.

50.   J. W. Wiench, B. Tischendorf, J. U. Otaigbe and M. Pruski, *J. Mol. Struct.*, 2002, **602**, 145-157.

51.   F. Fayon, C. Bessada, J. P. Coutures and D. Massiot, *Inorg. Chem.*, 1999, **38**, 5212-5218.

52.   C. Roiland, F. Fayon, P. Simon and D. Massiot, *J. Non-Cryst. Solids*, 2011, **357**, 1636-1646.

53.   J. W. Wiench, M. Pruski, B. Tischendorf, J. U. Otaigbe and B. C. Sales, *J. Non-Cryst. Solids*, 2000, **263**, 101-110.

54.   F. Fayon, C. Roiland, L. Emsley and D. Massiot, *J. Magn. Reson.*, 2006, **179**, 49-57.

55.   D. R. Neuville, L. Cormier and D. Massiot, *Geochim. Cosmochim. Ac.*, 2004, **68**, 5071-5079.

56.   Y. Zhang, S. Mukherjee and E. Oldfield, *J. Am. Chem. Soc.*, 2005, **127**, 2370-2371.

57.   Y.-I. Kim, S. Cadars, R. Shayib, T. Proffen, C. S. Feigerle, B. F. Chmelka and R. Seshadri, *Phys. Rev. B*, 2008, **78**, 195205-195217.

58.   K. H. Mroue and W. P. Power, *J. Phys. Chem., A*, 2010, **114**, 324-335.

59.   A. S. Lipton, M. D. Smith, R. D. Adams and P. D. Ellis, *J. Am. Chem. Soc.* 2002, **124**, 410-414.

60.   S. Sham and G. Wu, *Can. J. Chem.*, 1999, **77**, 1782-1787.

61.   A. Sutrisno, L. Liu, J. Xu and Y. Huang, *Phys. Chem. Chem. Phys*, 2011, **13**, 16606-16617.

62.   D. Laurencin, A. Wong, R. Dupree and M.E. Smith, *Magn. Reson. Chem.*, 2008, 46, 347-350

63.   C. Gervais, D. Laurencin, A. Wong, F. Pourpoint, J. Labram, B. Woodward, A. P. Howes, K. J. Pike, R. Dupree, F. Mauri, C. Bonhomme and M. E. Smith, *Chem. Phys. Lett.*, 2008, **464**, 42-48.

64.   U. Hoppe, R. Kranold, D. Stachel, A. Barz and A. C. Hannon, *Z. Naturforsch. A*, 2000, **55**, 369-380.

65.   U. Hoppe, *J. Non-Cryst. Solids*, 1996, **195**, 138-147.

66.   S. Bruni, F. Cariati, A. Corrias, P. H. Gaskell, A. Lai, A. Musinu and G. Piccaluga, *J. Phys. Chem.*, 1995, **99**, 15229-15235.

67.   G. Navarra, A. Falqui, G. Piccaluga and G. Pinna, *Phys. Chem. Chem. Phys.*, 2002, **4**, 4817-4822.

68.   K. Suzuya, K. Itoh, A. Kajinami and C. K. Loong, Journal *J. Non-Cryst. Solids*, 2004, **345**, 80-87.

69.   F. Döhler, A. Mandlule, L. van Wüllen, M. Friedrich and D. S. Brauer, *J. Mater Chem. B*. 2015, **3**, 1125-1134.

70.   B.C. Bunker, G.W. Arnold and J.A. Wilder, *J. Non-Cryst. Solids*, 1984, **64**, 291-316.

71.   H. S. Gao, T. N. Tan and D. H. Wang, *J. Control. Release*, 2004, **96**, 29-36.

72.   R.G. Hill, Private Communication.

73.   V. Salih, A. Patel and J. C. Knowles, *Biomed. Mater.*, 2007, **2**, 11-20.

74.   *CRC Handbook of Chemistry and Physics, 89th Edition*, D. R. Lide Ed., CRC Press/Taylor and Francis, Boca Raton, FL.,USA.

75.   P. Boussard, P.E.M. Siegbahn and U. Wahlgren in "*Adsorption of Ionic Solids and Thin Films*" Springer Thin Film Series Surface Sciences, 1993, **33**, 192.

76.   C. Calvo, *Can. J. Chem.*, 1965, **43**, 436-445.

77.   J.S. Stephens and C. Calvo, *Can. J. Chem.*, 1967, **45**, 2303-2312.

78.   C. Calvo, *J. Phys. Chem. Solids*, 1963, **24**, 141-149.

79.   T. Bataille, P.Benard-Rocherulle, and D. Louer, *J. Solid State Chem.*, 1998, **140**, 62-70.

80.   O.V. Karimova, O.V. Yakubovich and V.S. Urusov, *Vest. Mosk. Univ. Geol*. 1997, **52**, 35-45.

23

81.   B.E. Robertson and C. Calvo, *J. Solid State Chem.*, 1970, **1**, 120-133.

82.   C. Calvo, *Can. J. Chem.*, 1965, **43**, 1147-1153

83.   M.T. Averbuch-Pouchot, A. Durif, M. Bagieu Beucher, *Acta Crystallogr. Sect. C: Cryst. Struct. Commun.*, 1983, **39**, 25-26.

84.   M. Weil, *Acta Crystallogr., Sect. C: Cryst. Struct. Commun.* 2004, **60**, i20-i22.

85.   C. Baez-Doelle, D. Stachel, I. Svoboda and H. Fuess, *Z. Kristallogr.*, 1993, **203**, 282-283.

86.   M. Weil and R. Glaum, Eur. *J. Solid State Inorg. Chem.*, 1998, **35**, 495-508.

24

Table 1 Crystallographic density (ρ), percentage free volume ($\%V_{free}$), metal to phosphorus ratio (M/P), average phosphorus speciation (Av. Q^n) and zinc coordination number (CN_{Zn}) for crystalline zinc phosphates.

Phase	M/P	Av. Q^n	ρ (g cm^{-3})	$\%V_{free}$	CN_{Zn}	Ref
α-Zn$_3$(PO$_4$)$_2$	1.50	0	3.85	45.4	4	76
β-Zn$_3$(PO$_4$)$_2$	1.50	0	4.22	40.2	6	77
γ-Zn$_3$(PO$_4$)$_2$	1.50	0	3.96	43.8	6	78
γ-Zn(P$_2$O$_7$)	0.50	1	3.72	42.6	6	79
α-Zn(P$_2$O$_7$)	0.50	1	4.17	35.7	6	80
α-Zn(P$_2$O$_7$)	0.50	1	4.20	35.3	6	81
β-Zn(P$_2$O$_7$)	0.50	1	4.25	34.5	6	82
α-Zn(PO$_3$)$_2$	0.33	2	3.64	34.2	6	83
β-Zn(PO$_3$)$_2$	0.33	2	3.13	43.5	4	84
ZnP$_4$O$_{11}$	0.25	2.25	2.96	41.2	6	85
ZnP$_4$O$_{11}$	0.25	2.25	3.06	38.4	6	86

25

Table 2 Fitted and derived ^{31}P MAS-NMR parameters for glasses in the system 10Na$_2$O:(20 + x/2)ZnO:(20 + x/2)CaO:(50 − x) P$_2$O$_5$. Estimated standard deviations on isotropic chemical shifts are given in parentheses.

x	Q^n	δ_{iso} /ppm	$\Delta\delta$ ($\pm$ 5) /ppm	η ($\pm$ 0.05)	Rel. Int. ($\pm$ 2)/ %
0	Q^1	-9.52(12)	134	0.51	3
	Q^2	-26.15(1)	-193	0.45	76
	Q^2	-34.45(1)	-216	0.75	21
5	Q^1	-8.85(1)	130	0.59	18
	Q^2	-25.54(1)	-187	0.52	82
10	Q^1	-8.78(1)	128	0.58	47
	Q^2	-24.14(1)	-177	0.54	53
15	Q^0	5.17(1)	-101	0.00	3
	Q^1	-7.39(1)	123	0.63	77
	Q^2	-20.75(8)	-148	0.95	20
20	Q^0	5.20(2)	-52	0.00	26
	Q^1	-6.36(4)	120	0.64	74

Table 3. Intensity (%) of Q^n correlated species calculated by fitting the 1D MAS-NMR spectra with chemical shift and line widths, determined from the DQ MAS spectra.

x	$Q^{0,0}$	$Q^{0,1}$	$Q^{1,0}$	$Q^{1,1}$	$Q^{1,2}$	$Q^{2,1}$	$Q^{2,2}$
0	-	-	-	-	-	-	100.0
5	-	-	-	-	15.7	15.0	69.3
10	-	-	-	26.8	25.4	25.7	22.1
15	-	-	-	56.9	21.7	21.4	-
20	6.8	10.5	10.2	72.5	-	-	-

26

Table 4. ^{67}Zn NMR parameters extracted from a Czjzek simulation of the NMR spectra for glasses in the system $10Na_2O{:}(20 + x/2)ZnO{:}(20 + x/2)CaO{:}(50 - x)\,P_2O_5$.

x	C_Q ($\pm$ 0.5) / MHz	δ ($\pm$ 50) / ppm
0	7.4	150
5	7.4	235
10	8.0	190
15	7.7	220
20	7.8	200

Table 5. Structural parameters, r_{i-j} interatomic distance (Å) and N_{i-j} coordination number derived from fitted $T(r)$ for the studied glass compositions. Estimated standard deviations are given in parentheses.

x		P–NBO	P–BO	P–O (Total)	Zn–O[a]	Ca–O /Na–O (ave)	O–O
0	r_{i-j}	1.48(1)	1.60(1)		1.97(1)	2.31(1)	2.51(1)
	N_{i-j}	1.88(4)	1.88(4)	3.76	4.15(6)	7.00(10)	4.01(1)
5	r_{i-j}	1.50(1)	1.61(1)		1.96(1)	2.32(1)	2.51(1)
	N_{i-j}	2.49(10)	1.5(10)	3.99	4.0(6)	7.5(11)	3.87(1)
10	r_{i-j}	1.50(1)	1.61(1)		1.96(1)	2.33(1)	2.51(1)
	N_{i-j}	2.4(3)	1.35(1)	3.75	4.32(6)	7.52(10)	3.70(1)
15	r_{i-j}	1.51(1)	1.61(1)		1.97(1)	2.33(1)	2.51(1)
	N_{i-j}	2.71(1)	1.17(1)	4.05	3.9(4)	6.84(10)	3.57(1)
20	r_{i-j}	1.52(1)	1.61(1)		1.97(1)	2.36(1)	2.51(1)
	N_{i-j}	3.30(1)	0.75(1)	4.05	4.14(5)	6.84(12)	3.28(1)

[a]A second Zn-O distance at 2.17 Å was also fitted for the $x = 20$ composition.

27

Figures
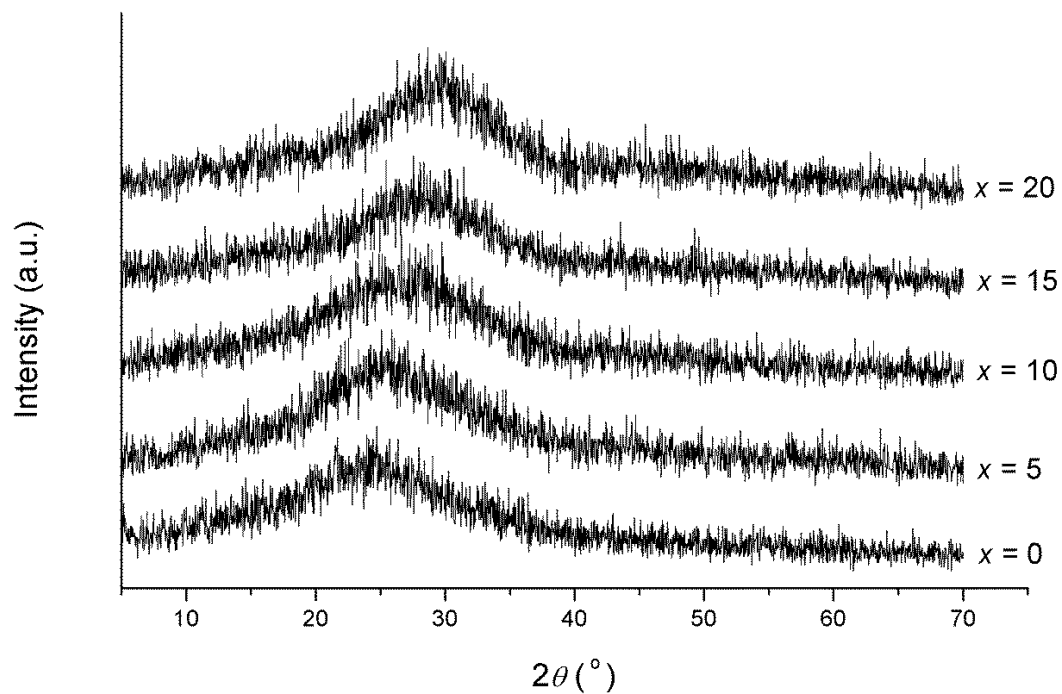
Fig. 1. X-ray diffraction patterns for glasses of composition $10Na_2O:(20 + x/2)ZnO:(20 + x/2)CaO:(50 - x)P_2O_5$.

28
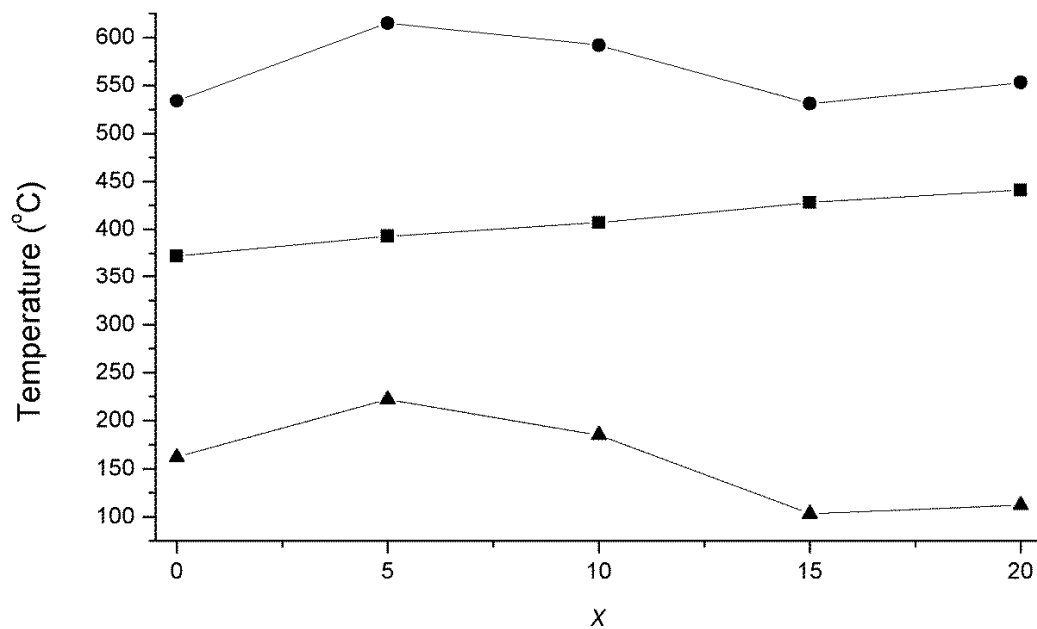
Fig. 2. Compositional variation of T_c (circles), T_g (squares) and $T_c - T_g$ (triangles) for glass compositions in the system $10Na_2O:(20 + x/2)ZnO:(20 + x/2)CaO:(50 - x)P_2O_5$. Lines are a guide to the eye.

29
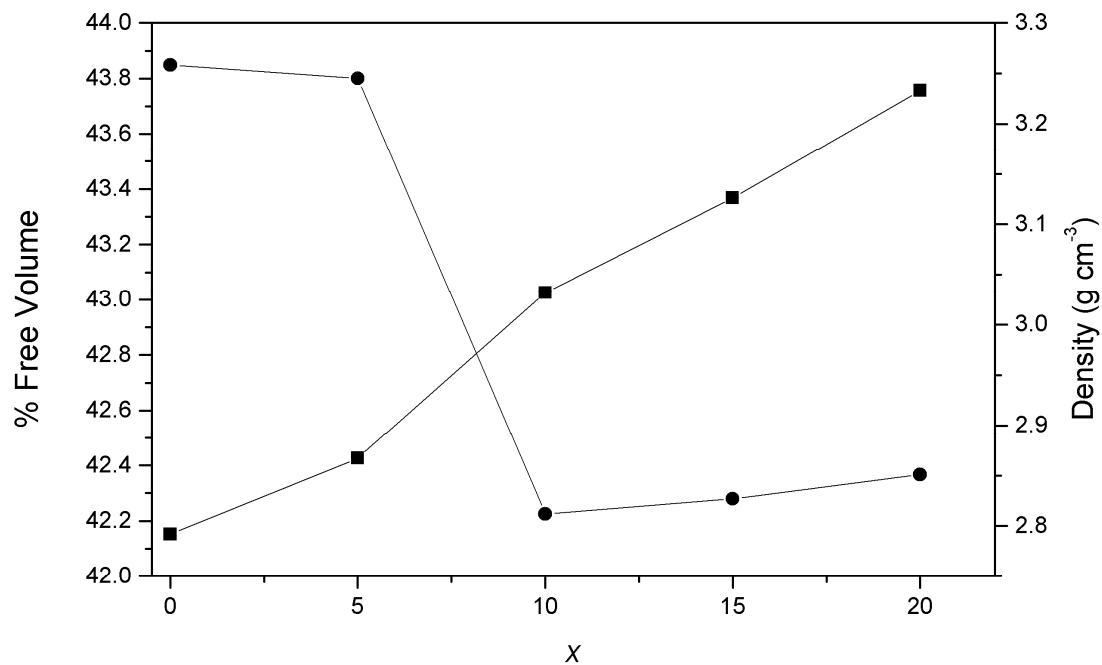
Fig. 3. Compositional variation of density (squares) and % free volume (circles) in the system $10Na_2O{:}(20 + x/2)ZnO{:}(20 + x/2)CaO{:}(50 - x)P_2O_5$.

30
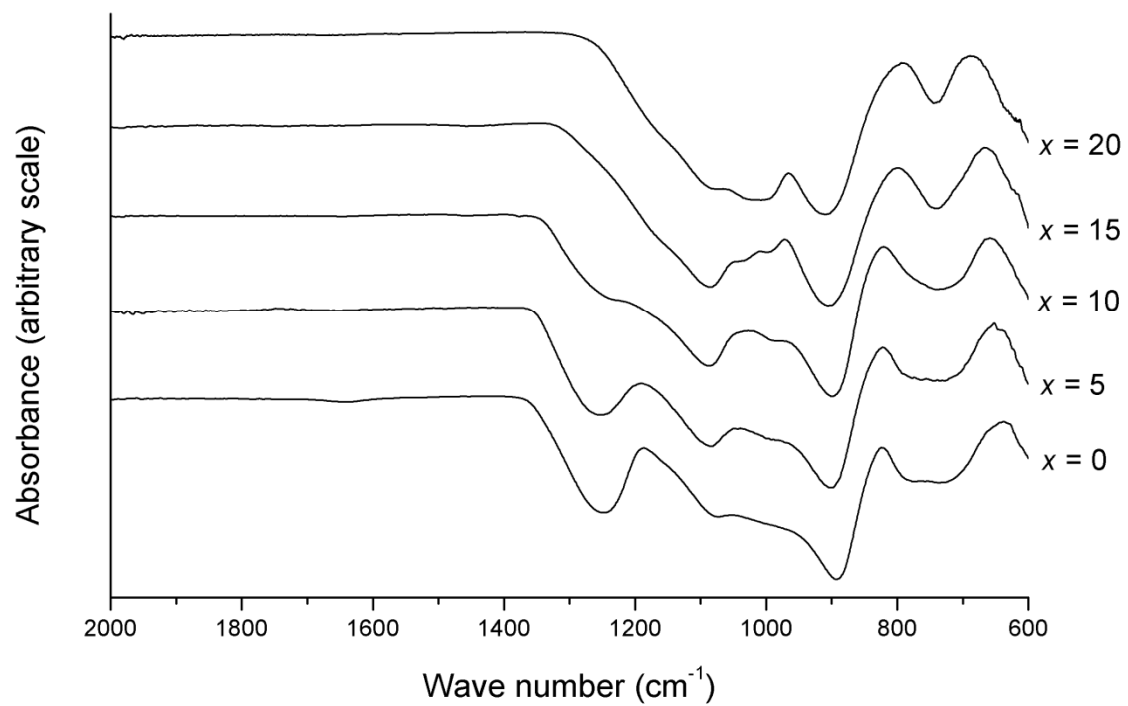
Fig. 4. FTIR spectra for the studied glass compositions.

31
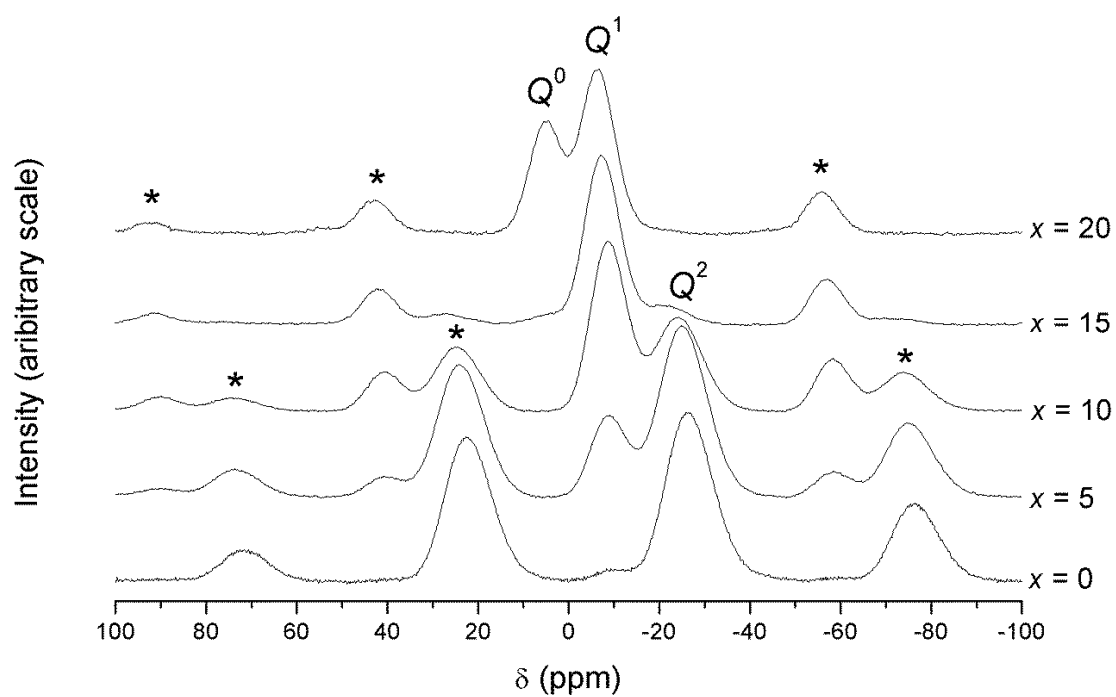
Fig. 5. Isotropic resonances in ^{31}P MAS-NMR spectra of glasses of composition $10Na_2O:(20 + x/2)ZnO:(20 + x/2)CaO:(50 - x)P_2O_5$ measured at 12 kHz spinning speed.

32
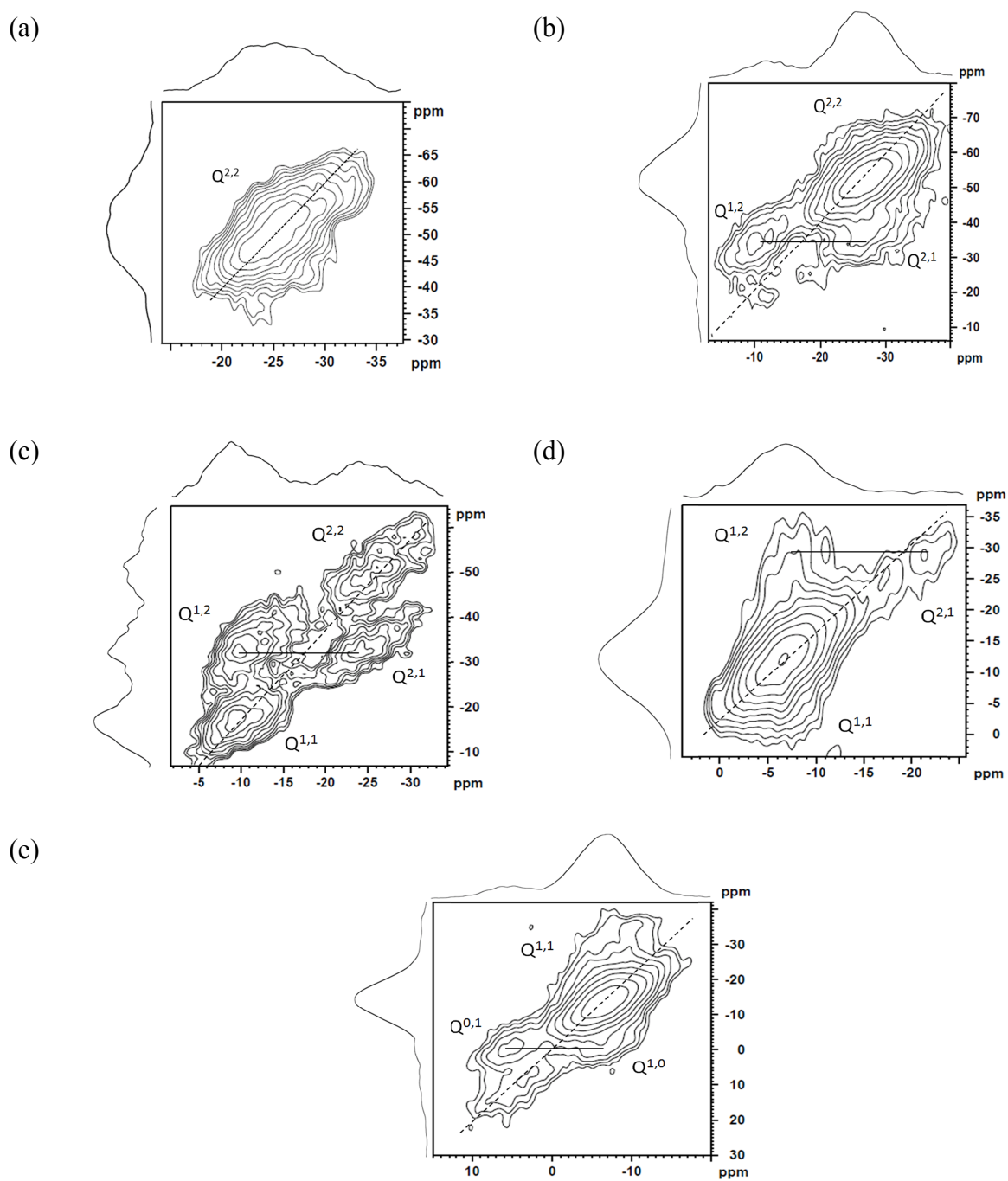
Fig. 6. ^{31}P-^{31}P DQ MAS-NMR spectra of studied glass compositions; (a) $x = 0$, (b) $x = 5$, (c) $x = 10$, (d) $x = 15$ and (e) $x = 20$. The lowest contour levels are set to 10% and levels increase in steps of 10%.

(a)

(b)
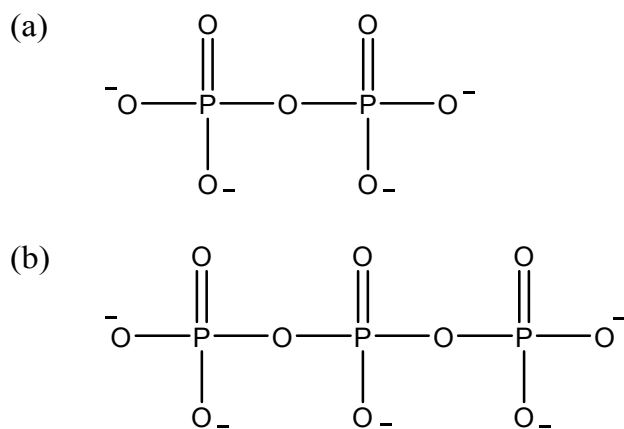
Fig. 7. Dimeric and trimeric phosphate anions (a) $(P_2O_7)^{4-}$ and (b) $(P_3O_{10})^{5-}$
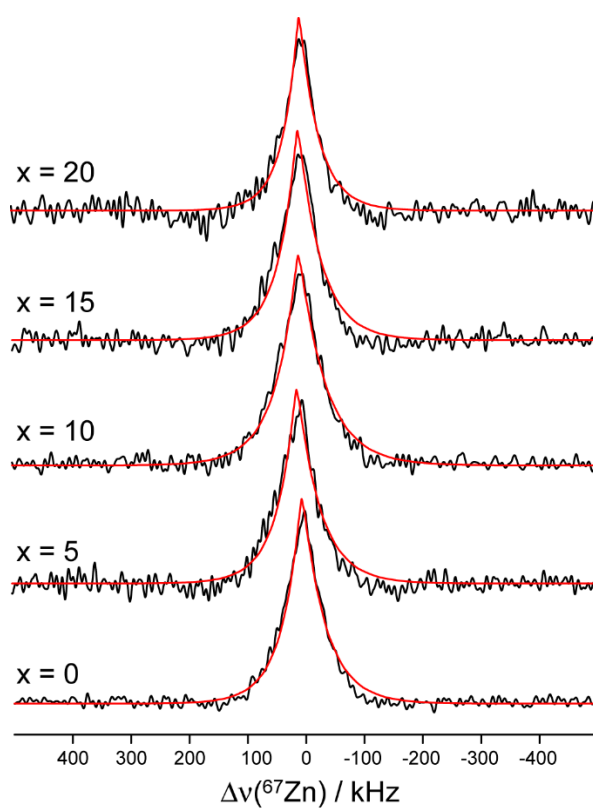
Fig. 8. ^{67}Zn NMR spectra are shown for glasses in the system $10Na_2O:(20 + x/2)ZnO:(20 + x/2)CaO:(50 - x) P_2O_5$ (in black) along with their Czjzek simulations. The simulation parameters are listed in Table 4.

34
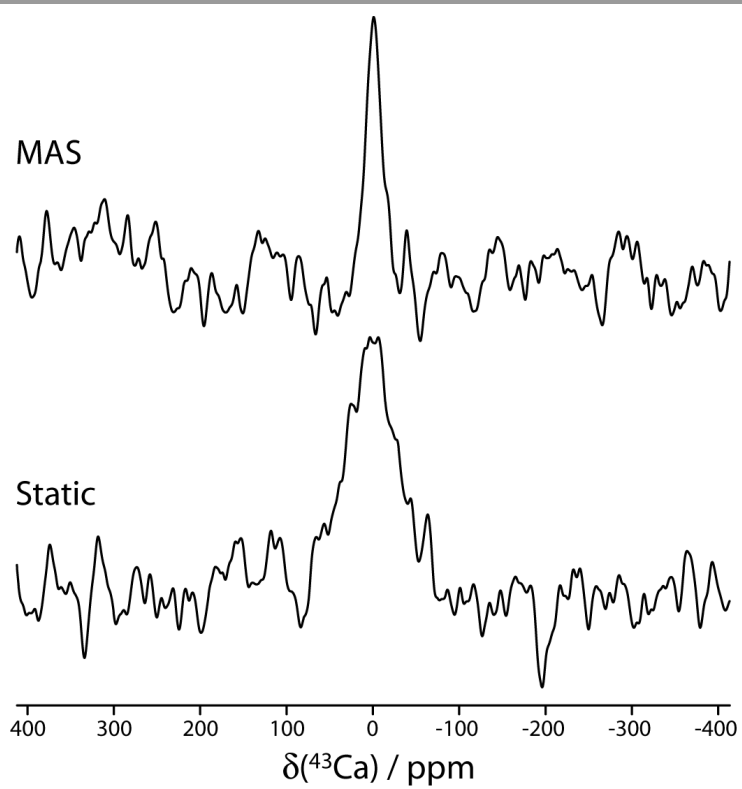
Fig. 9. ^{43}Ca static and MAS-NMR spectra for the $x = 15$ glass composition.

35
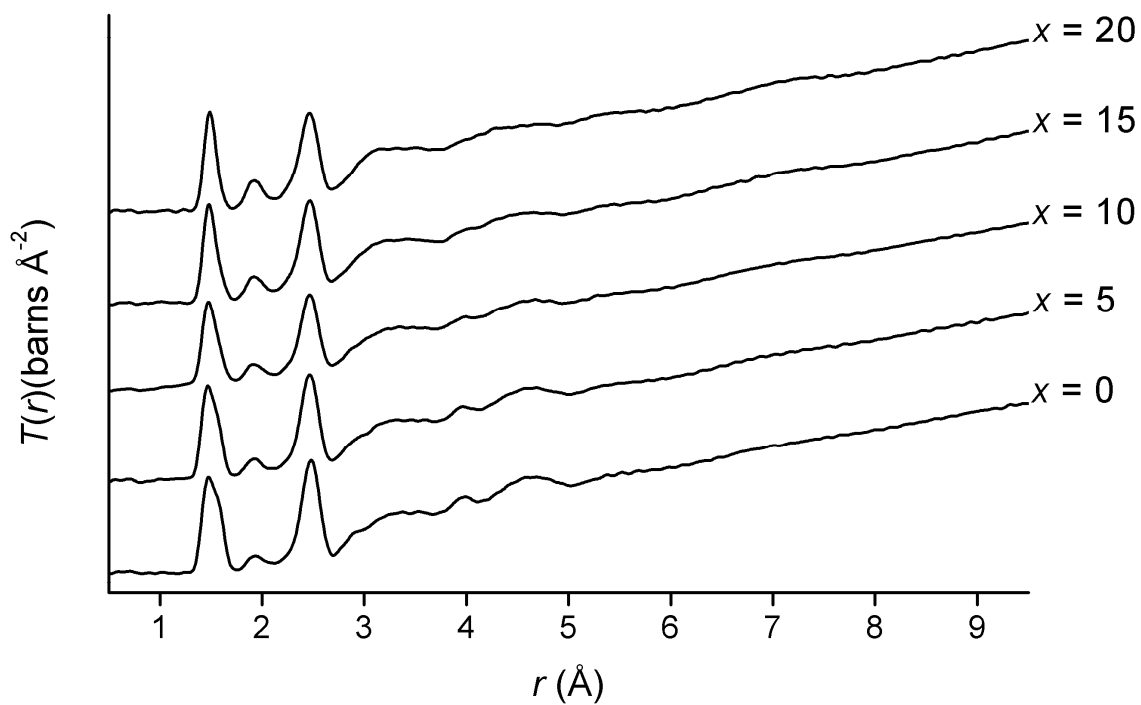
Fig. 10. Total correlation functions $T(r)$ for the studied glass compositions.

36
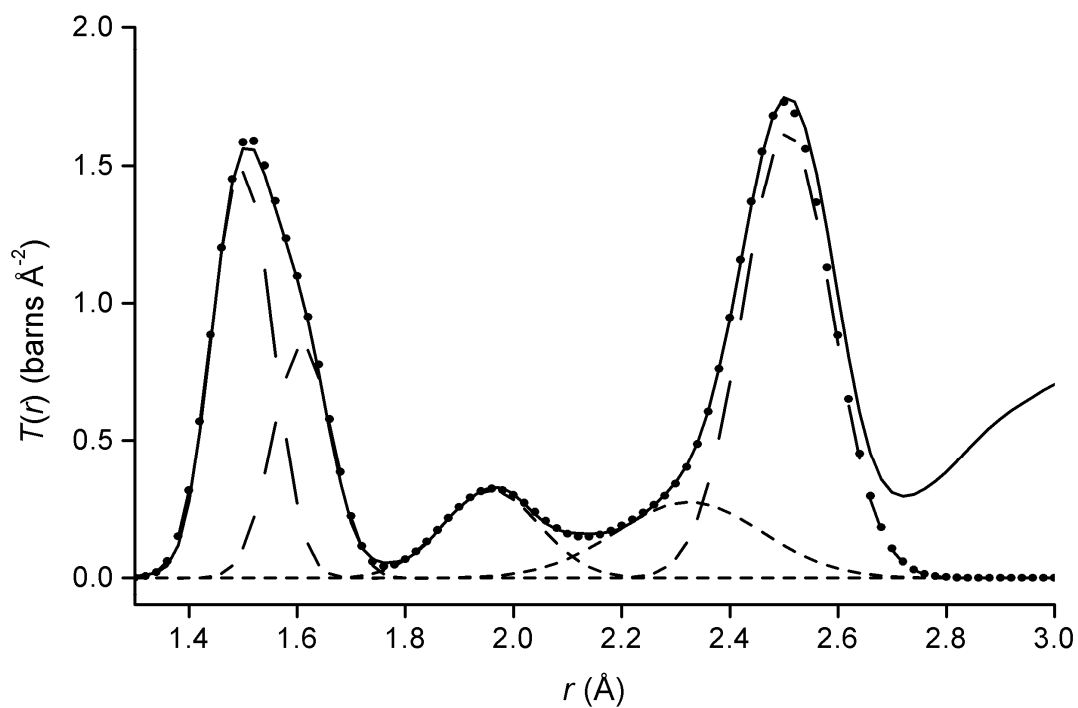
Fig. 11. Fitted total pair distribution function $T(r)$ (solid line) for the $x = 5$ composition. The individual pair distribution functions are shown by segmented lines.
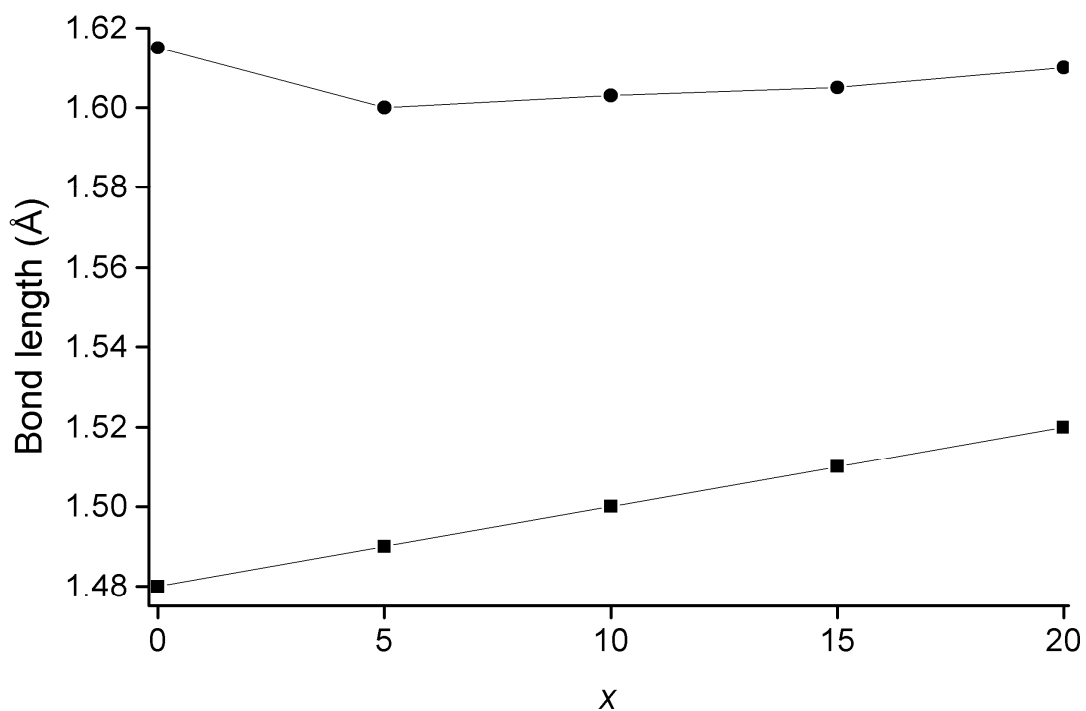
Fig. 12. Compositional variation of P–O bond lengths in glasses in the system $10Na_2O:(20 + x/2)ZnO:(20 + x/2)CaO:(50 - x)\ P_2O_5$, showing distances to bridging oxygen (P–BO) and non-bridging oxygen (P-NBO) atoms.

38

(a)

(b)
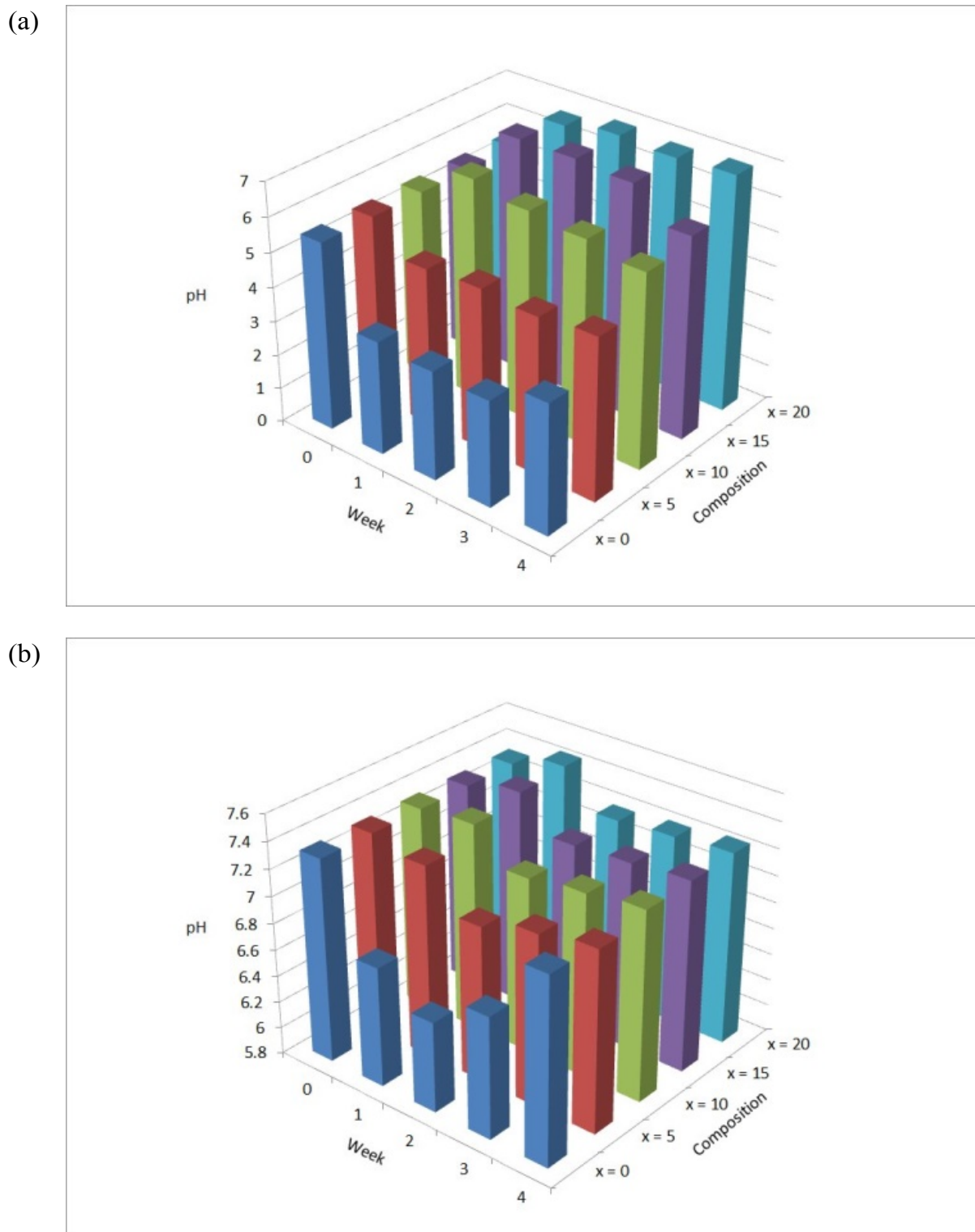
Fig. 13. pH changes of solution during solubility studies of studied glasses in (a) de-ionised water and (b) tris/HCl buffer

39

(a)
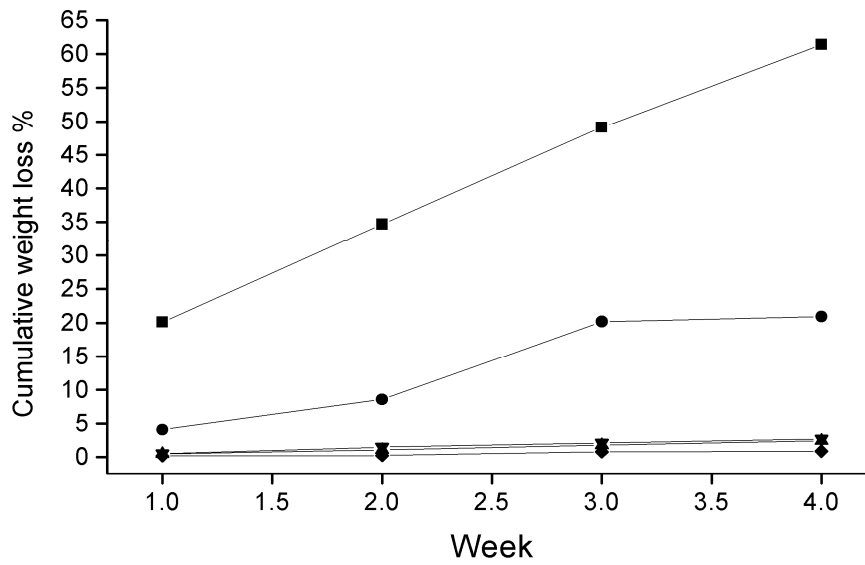
(b)
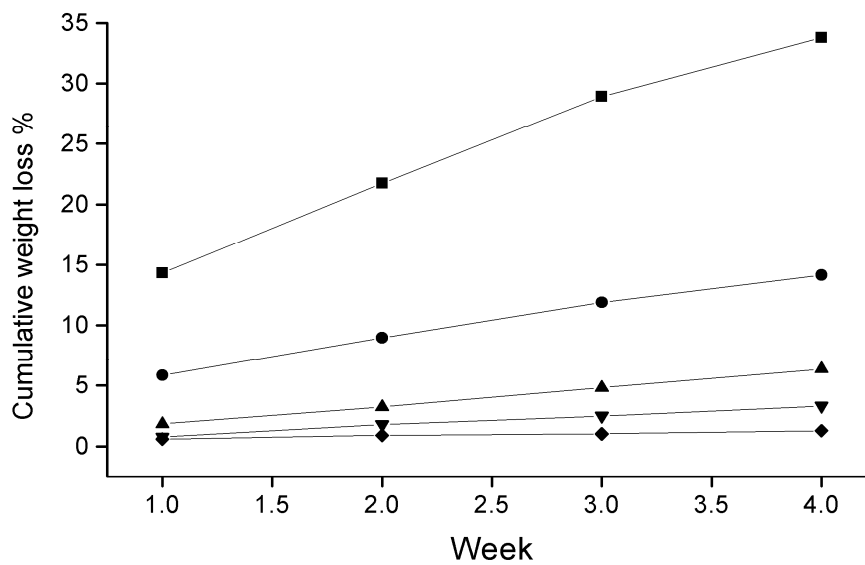
Fig. 14. Cumulative percentage weight loss of glass discs as a function of time in (a) de-ionised water and (b) tris/HCl buffer, showing $x = 0$ (squares), $x = 5$ (circles), $x = 10$ (up triangles), $x = 15$ (down triangles) and $x = 20$ (diamonds) compositions.
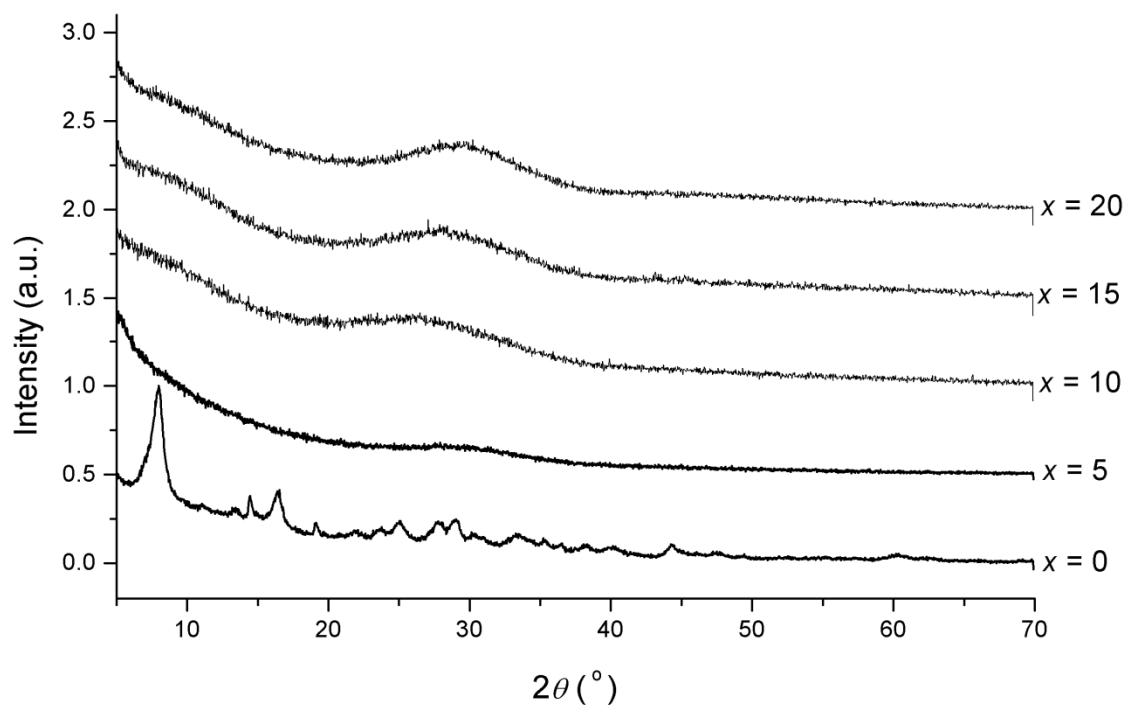
40

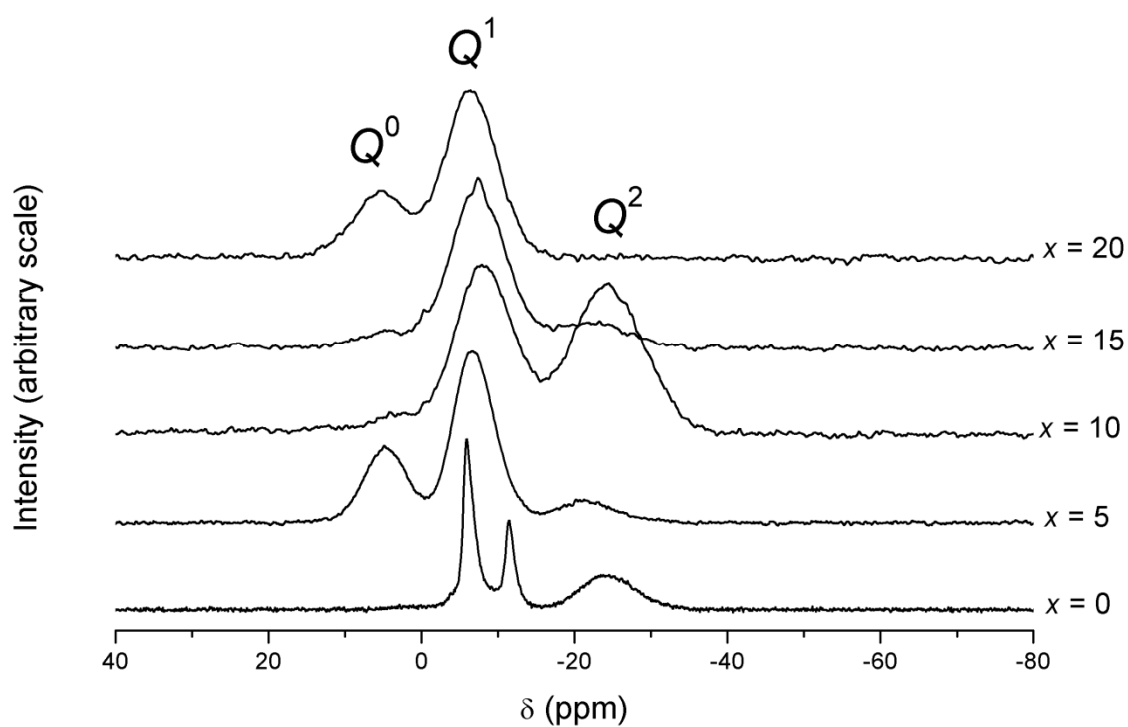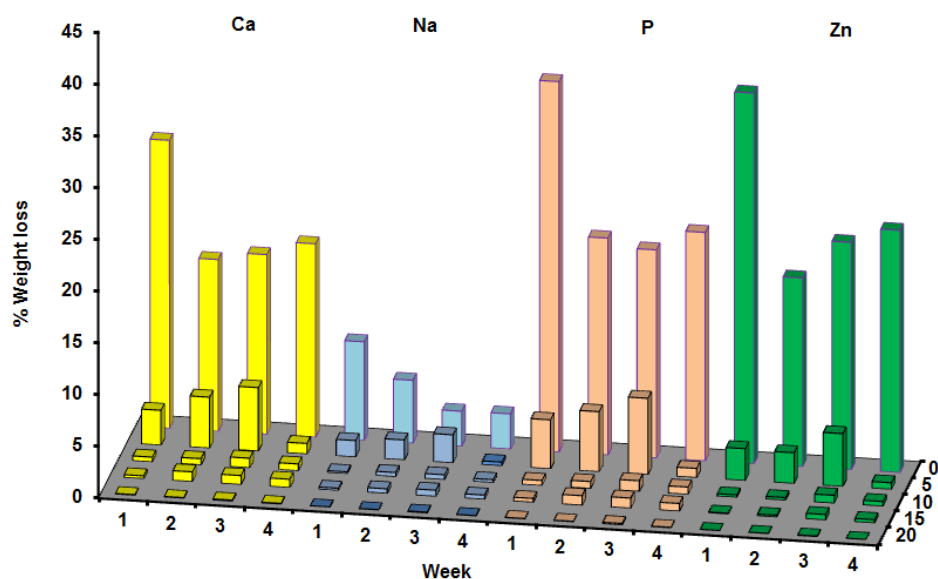Fig. 15. XRD patterns for studied glasses after immersion in tris/HCl buffer for 28 days.

Fig. 16. Isotropic resonances in ^{31}P MAS-NMR spectra of glasses of composition $10Na_2O\text{-}(20 + x/2)ZnO\text{-}(20 + x/2)CaO\text{-}(50 - x)P_2O_5$ after immersion for 28 days in tris/HCl buffer. Spectra were measured at 21 kHz spinning speed.
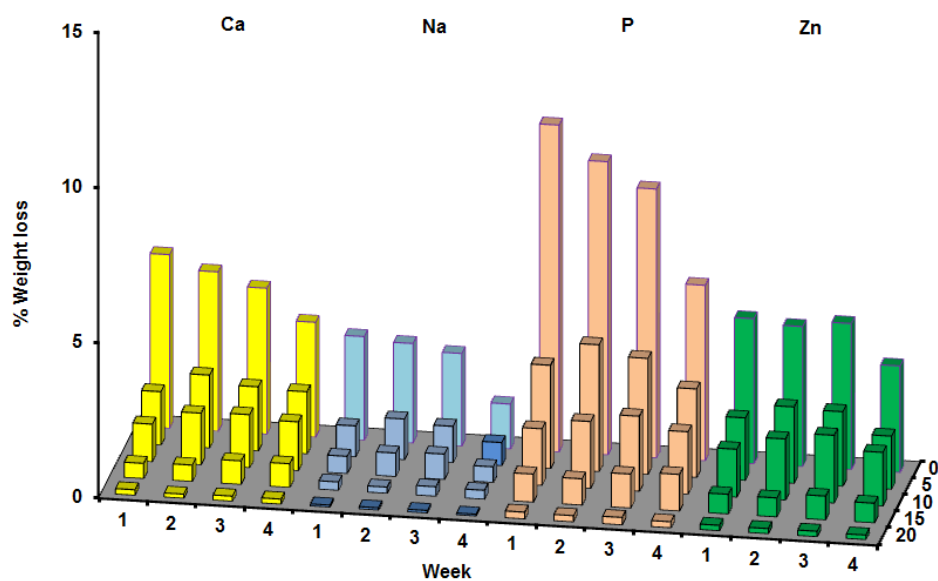
42

(a)

(b)

Fig. 17. Ion release profiles for studied glasses immersed in (a) deionised water and (b) tris/HCl buffer. Values are presented as percentage weight loss normalised to the ion content in the parent glass and with respect to the weight in the previous week.